

Constrained MRI using weighted Hilbert spaces: Fast scan-specific reconstruction with transparent assumptions

Chin-Cheng Chan¹ and Justin P. Haldar¹

¹Signal and Image Processing Institute, Ming Hsieh Department of Electrical and Computer Engineering, University of Southern California, Los Angeles, CA, United States

1 Introduction

The modern image reconstruction landscape contains various approaches that achieve different compromises between reconstruction performance, speed, transparency, and versatility/generalization:

- Data-driven learning methods achieve excellent performance on certain image quality metrics in typical cases, although can be black-box, data-hungry, and computation-intensive to train, and prone to hallucination,¹ resolution-loss,² and versatility concerns.³
- Principle-based regularization techniques also perform relatively well and can be more transparent with broader applicability/versatility, but can require computationally-expensive iterative algorithms.^{4–7}
- Scan-specific local-interpolation techniques like GRAPPA⁸ are fast and simple, although provide limited transparency and frequently-lower performance.

In this work, we introduce a novel technique that uses transparent scan-specific assumptions to achieve a favorable balance between performance, versatility, and computational complexity. Our approach uses a multichannel generalization of weighted Hilbert space interpolation,⁹ which allows us to impose prior information about the multichannel energy distribution and interchannel energy- and phase-correlations. The approach can be viewed from the perspective of Reproducing Kernel Hilbert Spaces (RKHSs),¹⁰ which enables computationally-simple GRAPPA-like k-space interpolation, but with better performance and more transparency.

2 Theory

Consider an ideal continuous k-space signal $f_\ell(\mathbf{k})$, $\ell = 1, \dots, L$, acquired using an L -channel array-coil ($\mathbf{f}(\mathbf{k}) \in \mathbb{C}^L$ in vector notation), with noisy multichannel k-space measurements $\mathbf{d}_m \in \mathbb{C}^L$, $m = 1, \dots, M$, made at sampling locations \mathbf{k}_m .

We propose to reconstruct continuous k-space from its samples by solving a minimum-norm reconstruction problem in a weighted Hilbert space⁹:

$$\hat{\mathbf{f}}(\mathbf{k}) = \arg \min_{\mathbf{f}(\mathbf{k})} \sum_{m=1}^M \|\mathbf{f}(\mathbf{k}_m) - \mathbf{d}_m\|_2^2 + \lambda \iint \mathbf{g}(\mathbf{x})^H \mathbf{W}^{-1}(\mathbf{x}) \mathbf{g}(\mathbf{x}) d\mathbf{x},$$

where the first term encourages data-consistency and the second term corresponds to the weighted Hilbert space norm. Here, $\mathbf{g}(\mathbf{x})$ is the L -channel image obtained via inverse Fourier transform of $\mathbf{f}(\mathbf{k})$, λ is a regularization parameter, and $\mathbf{W}(\mathbf{x})$ is a spatially-varying matrix function that defines the weighted Hilbert space, and captures the image behavior that we wish to promote. In the single-channel case,⁹ $\mathbf{W}(\mathbf{x})$ embodies assumptions about the expected spatial-energy distribution of $\mathbf{g}(\mathbf{x})$, with larger values of $\mathbf{g}(\mathbf{x})$ discouraged wherever $\mathbf{W}(\mathbf{x})$ is small. In the multichannel case, the diagonal elements of $\mathbf{W}(\mathbf{x})$ reflect the expected spatial-energy distributions of each channel, while the off-diagonal terms capture the expected energy- and phase-correlations between each channel pair. (For intuition, it may help to view $\mathbf{W}(\mathbf{x})$ as analogous to a spatially-varying multichannel covariance matrix for the image energy).

Importantly, this choice of norm imbues the weighted Hilbert space with RKHS structure,¹⁰ with shift-invariant kernel function

$$\mathcal{K}(\mathbf{k}, \mathbf{q}) \triangleq \iint \mathbf{W}(\mathbf{x}) e^{-i2\pi(\mathbf{k}-\mathbf{q}) \cdot \mathbf{x}} d\mathbf{x}.$$

RKHS structure means that, for any fixed k-space sampling pattern, the computation of $\hat{\mathbf{f}}(\mathbf{k})$ can be reframed as simple linear shift-invariant k-space interpolation (similar to GRAPPA), where the interpolation weights are simple functions of the kernel and sampling pattern.¹⁰

This approach is computationally simple, and the explicit use of $\mathbf{W}(\mathbf{x})$ provides full-transparency about the constraints we impose.

3 Methods

Experiments were conducted using 96 retrospectivelyundersampled T_2 -weighted multichannel brain datasets from the fastMRI database¹¹ ($4\times$ uniformundersampling with 16 central autocalibration (ACS) lines). Reconstructions were performed using conventional GRAPPA⁸, Residual RAKI¹² (a recent scan-specific neural-network approach), Autocalibrated LORAKS¹³ (a relativelyfast iterative regularization-based approach), and our proposed weighted Hilbert space approach. To mitigate hidden noise problems,¹⁴ denoising was used to obtain ground-truth images.

Our weighted Hilbert Space framework admits different ways of choosing $\mathbf{W}(\mathbf{x})$ to impose different constraints. We present illustrations for two cases that both derive $\mathbf{W}(\mathbf{x})$ from the ACS lines:

- **GRAPPA-Weights:** We estimate the empirical autocorrelation function from ACS data (similar to GRAPPA calibration⁸) and obtain $\mathbf{W}(\mathbf{x})$ via the Fourier transform.
- **LORAKS-Weights:** We use the nullspace vectors (corresponding to support and multichannel-correlation constraints) obtained from the LORAKS autocalibration process¹³ to define $\mathbf{W}^{-1}(\mathbf{x})$.

Examples are shown in Figures 1-2.

4 Results

As shown in Figures 3-4, the proposed method (LORAKS-weights) consistently outperformed conventional GRAPPA in normalized root-mean-squared error (NRMSE) and structural similarity (SSIM), even offering comparable performance to Autocalibrated LORAKS (i.e., the best-performing method in the comparison) but with $\sim 6 \times$ faster computation. The proposed method (LORAKS-weights) also consistently outperformed Residual RAKI (which was hampered by limited ACS) and the proposed method with GRAPPA-weights—not shown due to space constraints.

Figure 5 shows an example where the quality differences between methods were especially noticeable, also including computation-time information which demonstrates the speed of the proposed approach.

5 Conclusion

This work introduced a new weighted Hilbert space framework for reconstructing undersampled MRI data. The approach leverages the structure of RKHSs to perform reconstruction using transparent scan-specific constraints, offering NRMSE/SSIM performance that is similar to iterative regularization methods but with the computational simplicity of non-iterative interpolation, all while relying on simple priors with limited hallucination-risk. Although the approach was demonstrated for Cartesian imaging with energy-type constraints, it can also be used to impose other constraints (phase, transform-sparsity, etc.) and is compatible with non-Cartesian data.

6 Acknowledgments

This work was supported in part by NIH research grants U01-HL167613 and R01-MH116173, a USC Viterbi/Graduate School Fellowship, and computing resources from the USC Center for Advanced Research Computing.

7 References

- [1] Muckley MJ, Riemenschneider B, Radmanesh A, et al. Results of the 2020 fastMRI challenge for machine learning MR image reconstruction. *IEEE Trans. Med. Imaging*.

2021;40:2306-2317. doi:10.1109/TMI.2021.3075856.

- [2] Chan CC, Haldar JP. Local perturbation responses and checkerboard tests: Characterization tools for nonlinear MRI methods. *Magn. Reson. Med.* 2021;86:1873-1887. doi:10.1002/mrm.28828.
- [3] Wang J, Haldar JP. Can imaging still see the unseen in the age of AI? Implications for scientific discovery. In: Proc. Asilomar 2025; In Press.
- [4] Lustig M, Donoho D, Pauly JM. Sparse MRI: The application of compressed sensing for rapid MR imaging. *Magn. Reson. Med.* 2007;58:1182-1195. doi:10.1002/mrm.21391.
- [5] Liang ZP. Spatiotemporal imaging with partially separable functions. In: Proc. IEEE Int. Symp. Biomed. Imag.; 2007:988-991. doi:10.1109/ISBI.2007.357020.
- [6] Shin PJ, Larson PEZ, Ohliger MA, Elad M, Pauly JM, Vigneron DB, Lustig M. Calibrationless parallel imaging reconstruction based on structured low-rank matrix completion. *Magn. Reson. Med.* 2014;72:959-970. doi:10.1002/mrm.24997.
- [7] Haldar JP. Low-rank modeling of local k-space neighborhoods (LORAKS) for constrained MRI. *IEEE Trans. Med. Imaging.* 2014;33:668-681. doi:10.1109/TMI.2013.2293974.
- [8] Griswold MA, Jakob PM, Heidemann RM, Nittka M, Jellus V, Wang J, Kiefer B, Haase A. Generalized autocalibrating partially parallel acquisitions (GRAPPA). *Magn. Reson. Med.* 2002;47:1202-1210. doi:10.1002/mrm.10171
- [9] Haldar JP. Shannon-like interpolation with spectral priors and weighted Hilbert spaces: Beyond the Nyquist rate. arXiv:2410.21184. 2024. doi:10.48550/arXiv.2410.21184.
- [10] Paulsen VI, Raghupathi M. An introduction to the theory of reproducing kernel Hilbert spaces. Cambridge University Press; 2016. doi:10.1017/CBO9781316219232.
- [11] Knoll F, Murrell T, Sriram A, Yakubova N, Zbontar J, Rabbat M, Defazio A, Muckley MJ, Sodickson DK, Zitnick CL, Recht MP. Advancing machine learning for MR image reconstruction with an open competition: Overview of the 2019 fastMRI challenge. *Magn. Reson. Med.* 2020;84:3054-3070. doi:10.1002/mrm.28338.
- [12] Zhang C, Moeller S, Demirel OB, Uğurbil K, Akçakaya M. Residual RAKI: A hybrid linear and non-linear approach for scan-specific k-space deep learning. *NeuroImage.* 2022;256:119248. doi:10.1016/j.neuroimage.2022.119248.
- [13] Haldar JP. Autocalibrated LORAKS for fast constrained MRI reconstruction. In: Proc. IEEE Int. Symp. Biomed. Imag.; 2015:910-913. doi:10.1109/ISBI.2015.7164018.
- [14] Wang J, An D, Haldar JP. The "hidden noise" problem in MR image reconstruction.

8 Figures

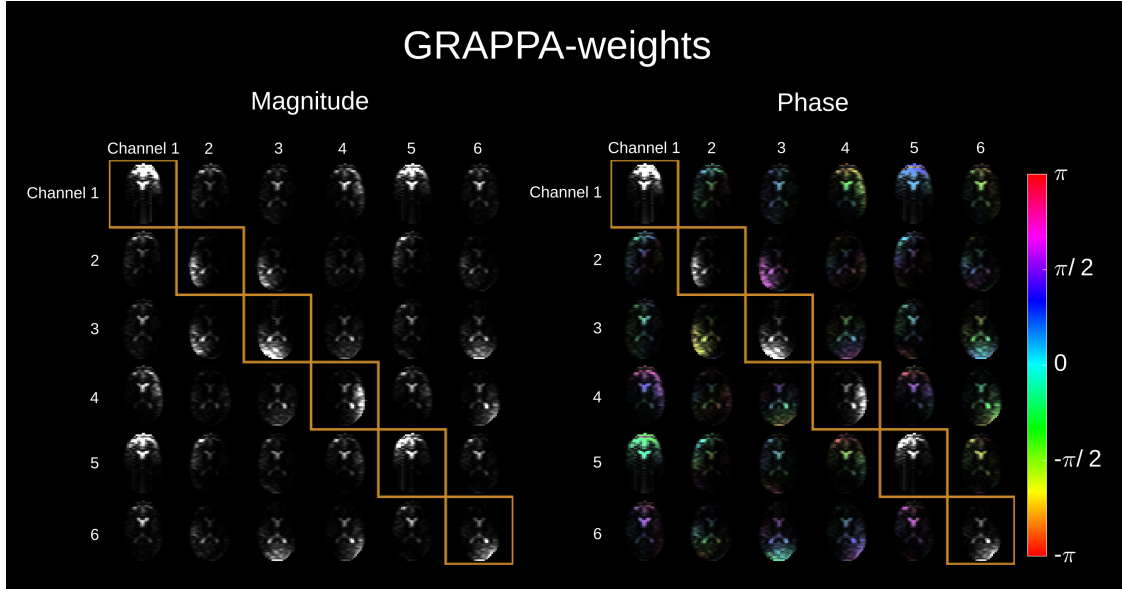


Figure 1: Representative $\mathbf{W}(\mathbf{x})$ corresponding to GRAPPA-weights. (For visualization, only 6 channels are shown). The (left) magnitude of $\mathbf{W}(\mathbf{x})$ represents assumptions about the (diagonal) energy distribution for each channel and (off-diagonal) cross-channel energy correlation, while the (right, off-diagonal) phase represents assumptions about cross-channel phase relationships.

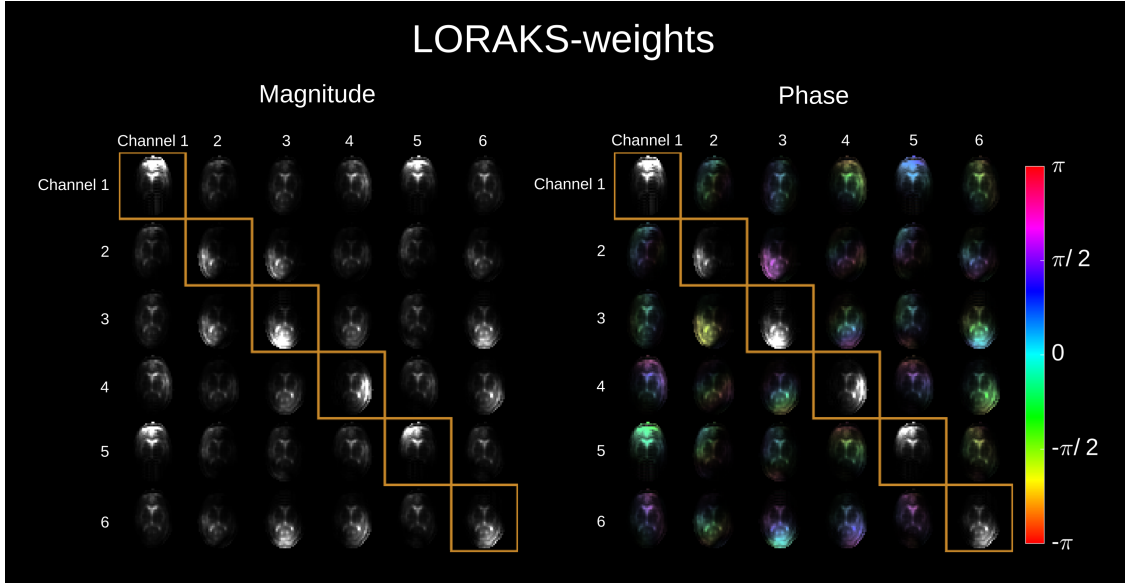


Figure 2: Representative $\mathbf{W}(\mathbf{x})$ corresponding to LORAKS-weights. (For visualization, only 6 channels are shown). The (left) magnitude of $\mathbf{W}(\mathbf{x})$ represents assumptions about the (diagonal) energy distribution for each channel and (off-diagonal) cross-channel energy correlation, while the (right, off-diagonal) phase represents assumptions about cross-channel phase relationships.

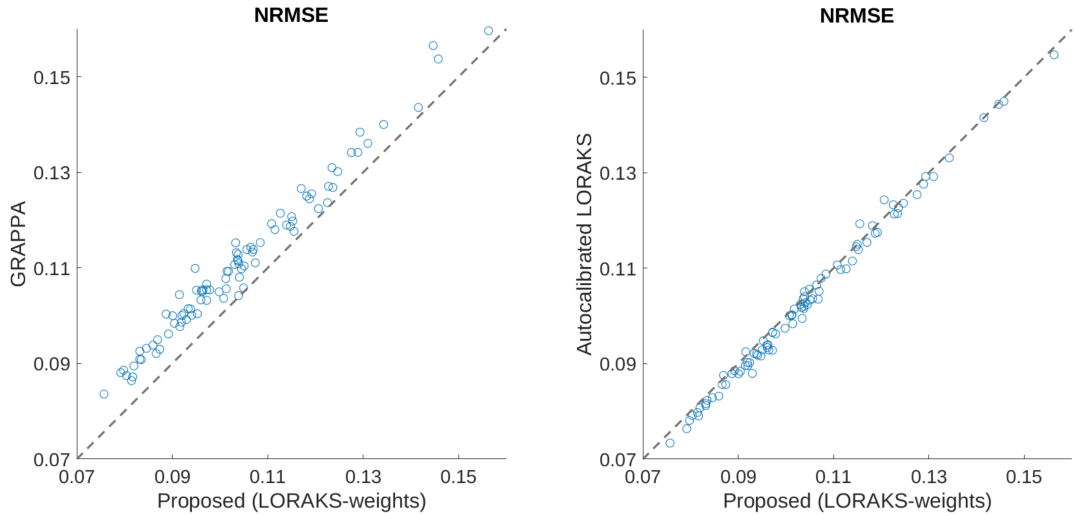


Figure 3: Scatter plots comparing NRMSE performance between (left) GRAPPA and the proposed method (LORAKS-weights) and (right) Autocalibrated LORAKS and the proposed method (LORAKS-weights) across 96 brain images. The proposed method offers improved performance when the points lie above the 45° line.

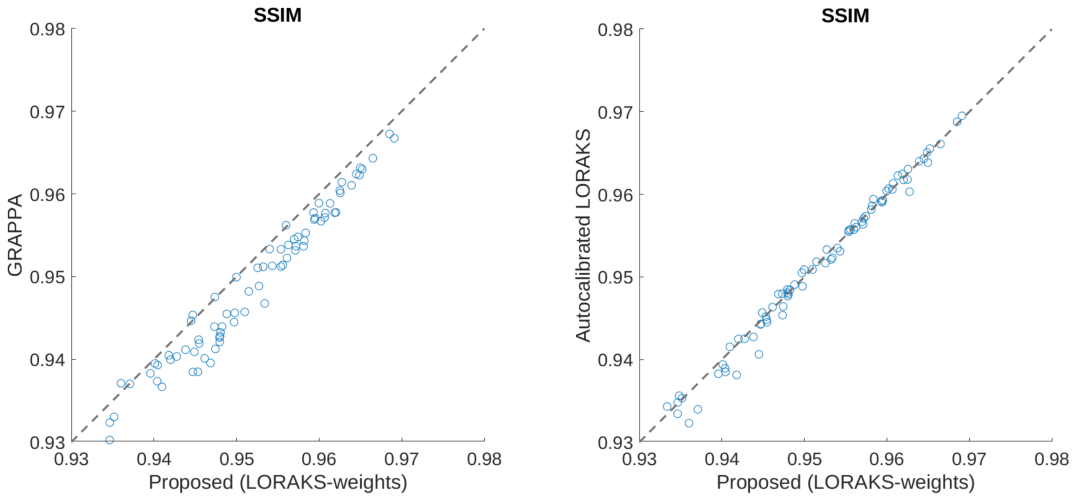


Figure 4: Scatter plots comparing SSIM performance between (left) GRAPPA and the proposed method (LORAKS-weights) and (right) Autocalibrated LORAKS and the proposed method (LORAKS-weights) across 96 brain images. The proposed method offers improved performance when the points lie below the 45° line.

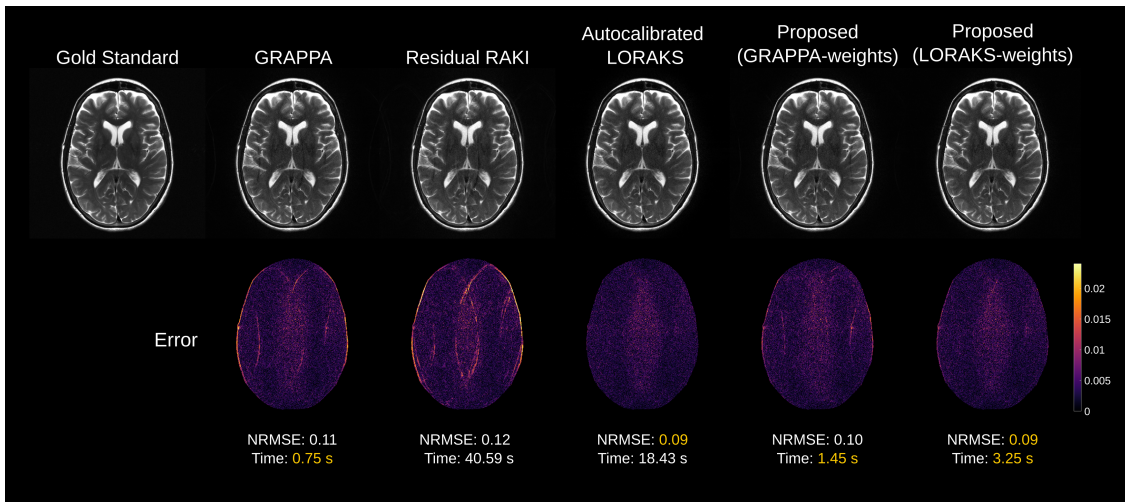


Figure 5: Illustrative reconstruction results and error maps from a single case, reflecting the error characteristics and NRMSE/speed performance characteristics described in the text.